*VOR (version of record)

Thermodynamic Analyses of Fuel Production via Solar-driven Ceria-based Non-stoichiometric Redox Cycling: A Case Study of the Isothermal Membrane Reactor System

Sha Li, Peter B. Kreider, Vincent M. Wheeler, and Wojciech Lipiński[1]

E-mail: wojciech.lipinski@anu.edu.au

Research School of Engineering,

The Australian National University,

Canberra, ACT 2601, Australia

Abstract

A thermodynamic model of an isothermal ceria-based membrane reactor system is developed for fuel production via solar-driven simultaneous reduction and oxidation reactions. Inert sweep gas is applied on the reduction side of the membrane. The model is based on conservation of mass, species and energy along with the Gibbs criterion. The maximum thermodynamic solar-to-fuel efficiencies are determined by simultaneous multivariable optimization of operational parameters. The effects of gas heat recovery and reactor flow configurations are investigated. The results show that maximum efficiencies of 1.3% (3.2%) and 0.73% (2.0%) are attainable for water splitting (carbon dioxide splitting) under counter- and parallel-flow configurations, respectively, at an operating temperature of 1900 K and 95% gas heat recovery effectiveness. In addition, insights on potential efficiency improvement for the membrane reactor system are further suggested. The efficiencies reported are found to be much lower than those reported in literature. We demonstrate that the thermodynamic models reported elsewhere can violate the Gibbs criterion and, as a result,

[1]Corresponding author.

lead to unrealistically high efficiencies. The present work offers enhanced understanding of the counter-flow membrane reactor and provides more accurate upper efficiency limits for membrane reactor systems.

1. Introduction

Solar-driven, two-step, non-stoichiometric metal oxide redox cycling offers an appealing pathway to produce renewable fuels from water and/or carbon dioxide [1,2]. A two-step redox cycle for water (Eq. (2)) or carbon dioxide (Eq. (3)) splitting comprises an endothermic reduction step

$$\frac{1}{\Delta\delta}\mathrm{M}_x\mathrm{O}_{y-\delta_{\mathrm{ox}}} \rightarrow \frac{1}{\Delta\delta}\mathrm{M}_x\mathrm{O}_{y-\delta_{\mathrm{red}}} + \frac{1}{2}\mathrm{O}_2, \tag{1}$$

and an exothermic oxidation step to produce hydrogen (Eq. (2)) or carbon monoxide (Eq. (3))

$$\frac{1}{\Delta\delta}\mathrm{M}_x\mathrm{O}_{y-\delta_{\mathrm{red}}} + \mathrm{H}_2\mathrm{O(g)} \rightarrow \frac{1}{\Delta\delta}\mathrm{M}_x\mathrm{O}_{y-\delta_{\mathrm{ox}}} + \mathrm{H}_2, \tag{2}$$

$$\frac{1}{\Delta\delta}\mathrm{M}_x\mathrm{O}_{y-\delta_{\mathrm{red}}} + \mathrm{CO}_2 \rightarrow \frac{1}{\Delta\delta}\mathrm{M}_x\mathrm{O}_{y-\delta_{\mathrm{ox}}} + \mathrm{CO}, \tag{3}$$

where $\mathrm{M}_x\mathrm{O}_{y-\delta_{\mathrm{red}}}$ and $\mathrm{M}_x\mathrm{O}_{y-\delta_{\mathrm{ox}}}$ represent the reduced and oxidized metal oxides and $\Delta\delta = \delta_{\mathrm{red}} - \delta_{\mathrm{ox}}$ is the non-stoichiometry swing of the redox material between the reduced and oxidized states.

The fuel output is proportional to the change in non-stoichiometry, which can be achieved via temperature swing [3–7] or isothermal pressure swing [8–12] operating conditions. To produce the fuel continuously, both the reduction and oxidation steps need to proceed simultaneously. This can be achieved by a two-reactor system using stationary reactive material [7,13,14] or a single reactor system using a moving reactive material [15–17]. Alternatively, the continuous

fuel production can be achieved using an isothermal membrane reactor [18–21] by removing the oxygen generated via water or carbon dioxide thermolysis from the oxidation side of the membrane to the reduction side instantaneously. This in-situ fuel-production/separation process relies on the ion-conducting or mixed ionic-electronic conducting characteristics of an oxygen permeation membrane (OPM) and is driven by the oxygen chemical potential gradient across the membrane. This membrane reactor concept allows for both steps to proceed simultaneously and continuously at steady state using a stationary membrane and greatly simplifies the reactor design. Recently, this concept was demonstrated by Tou et al. [22] for solar-driven thermochemical splitting of CO_2 using a ceria-based membrane reactor.

Most of the studies on isothermal membrane reactors are focused on kinetic aspects and investigate the oxygen transport process across the membrane for identification of the rate-limiting step [23–26]. Very limited efforts have been made to understand the membrane reactor from a thermodynamic perspective [21,27]. Understanding the thermodynamic efficiency of the membrane reactor can offer insight on the future commercialization viability of this technology. Wang et al. [21] predicted the efficiency of a pump-assisted membrane reactor for water splitting by expanding on an oxygen permeation flux model developed in Ref. [24]. However, their thermodynamic model assumes constant oxygen partial pressure everywhere along the flow path on the reduction side, which may violate the law of mass conservation and can consequently overpredict the efficiency; when the oxygen is transported from the oxidation side to the reduction side, the oxygen partial pressure on the reduction side should increase. Zhu et al. [27] developed a thermodynamic model for a ceria-based membrane reactor system to produce CO and predicted an efficiency of over 10% at 1800 K with 95% gas heat recovery condition. Though their work is pioneering in offering an efficiency upper limit for the membrane reactor, the base assumption of

chemical equilibrium being enforced at both reactor inlet and outlet in their model is not justified, and leads to a model that violates the second law of thermodynamics [28,29]. Generally, enforcing equilibrium at a certain thermodynamic state does not necessarily ensure the reaction spontaneity at all thermodynamic states within a reaction system.

Expanding upon our recent studies [28,29], here we offer a thermodynamic analysis for the case of an isothermal membrane reactor system with reduction proceeding under the option of inert gas sweeping. Ceria is used as the membrane material. Two ideal plug flow configurations are considered: counter flow (CF) and parallel flow (PF) configurations. We aim to offer more realistic efficiency upper limits for the membrane reactor system under both flow configurations. This is achieved by: (*i*) ensuring the reaction spontaneity of both reduction and oxidation steps everywhere within the membrane reactor using Gibbs' criterion, and (*ii*) simultaneous multivariable optimization of operating parameters using efficiency as the objective function.

2. Methodology

A schematic of the membrane reactor system under study for water splitting is shown in Fig. 1. The system consists of a gas separator (GS), an isothermal membrane reactor and two gas–gas heat exchangers ($HX_{g,red}$ and $HX_{g,ox}$), with the first component termed as the work subsystem and the latter three as the heating subsystem. Concentrated solar power $\dot{Q}_{solar}$ is employed to provide both the heating requirement $\dot{Q}_{solar,h}$ and the penalty work requirement $\dot{Q}_{solar,pw}$ to each subsystem. The reactor is isobaric at 101325 Pa. Circled numbers from 1 to 12 signify thermodynamic states. The processes that cause the changes to a thermodynamic state will be represented by the notation (initial state → final state) in the following description.

Ambient air is supplied to the GS to produce the sweep gas (1→2, 3) for the reduction zone. The sweep gas is then preheated in the $HX_{g,red}$ from T_2 to T_4 (2→4) by the hot effluent gases which are cooled from T_6 to T_7 (6→7). Part of the solar power input supplied to the heating subsystem ($\dot{Q}_{solar,h}$) may be required to further preheat the sweep gas to T_5 ($\dot{Q}_{sg,h}$) if T_4 is lower than T_5 (4→5). In the case of hydrogen production, water is employed as the oxidizer to the oxidation zone. It is first preheated in the $HX_{g,ox}$ by the hot gas mixture after oxidation, resulting in T_9 and T_{12} for the inlet and outlet gases (8→9 and 11→12), respectively. A fraction of $\dot{Q}_{solar,h}$ will be required to further preheat water ($\dot{Q}_{H_2O,h}$) to the temperature of membrane reactor T_{10} (9→10). Another fraction of $\dot{Q}_{solar,h}$ is used to drive the water splitting in the isothermal membrane reactor ($\dot{Q}_{chem,WT}$). The rest of $\dot{Q}_{solar,h}$ is lost via re-radiation ($\dot{Q}_{rerad}$) as well as conduction and convection ($\dot{Q}_{other}$).

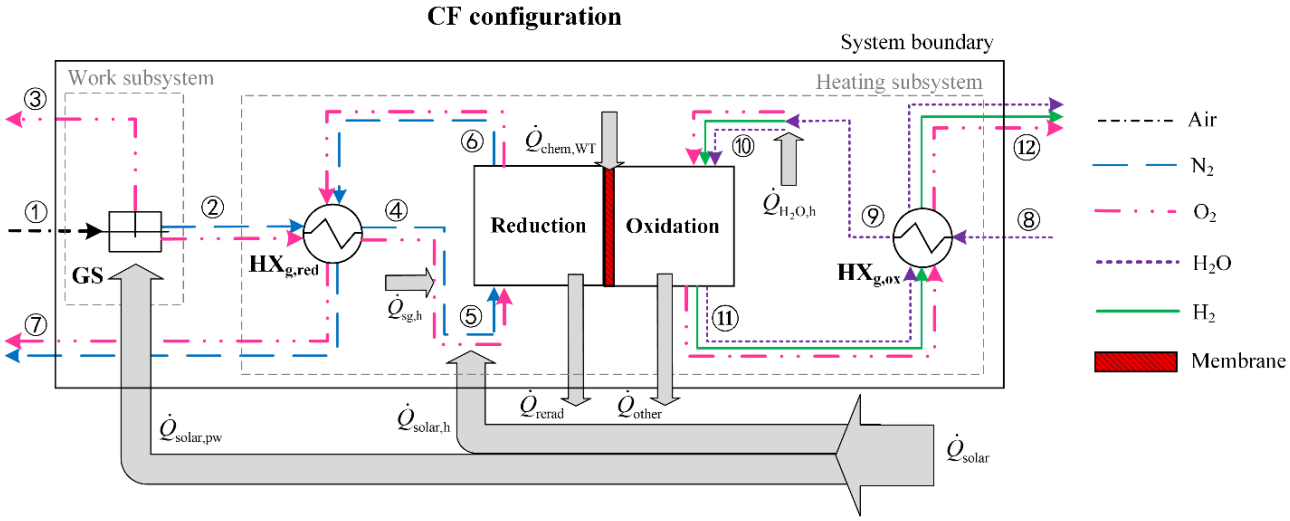

Fig. 1 Schematic of mass and energy flow of an isothermal membrane reactor system under the CF configuration for water splitting. Mass flow is indicated by thin arrows and energy flow by thick, gray arrows. An energy flow line pointing to or from a mass flow line indicates a heat addition or removal step, respectively.

2.1 System-level analysis

A detailed thermodynamic model has been described in a previous study [29] for a conventional redox reactor system. Herein, we apply the same methodology to the membrane reactor scenario. Many of the detailed equations in this work will remain unchanged or follow the same format with the only difference being the numbered thermodynamic states. In the following analysis, we will present a general overview of the thermodynamic model and only highlight changes necessary to adapt the previous model to the membrane reactor system.

Besides the assumptions made in the previous thermodynamic model, an additional assumption is introduced to the present work: the membrane of the reactor is so thin that the oxygen bulk diffusion across the membrane is fast enough that the non-stoichiometry gradient across the membrane can be neglected. The performance metric of the whole system is characterized by the solar-to-fuel efficiency as defined by [29]:

$$\eta = \frac{\dot{n}_{\mathrm{H_2}} \mathrm{HHV}_{\mathrm{H_2}}}{\dot{Q}_{\mathrm{solar,h}} + \dot{Q}_{\mathrm{solar,pw}}}, \tag{4}$$

where $\mathrm{HHV}_{\mathrm{H_2}}$, $\dot{n}_{\mathrm{H_2}}$, $\dot{Q}_{\mathrm{solar,h}}$ and $\dot{Q}_{\mathrm{solar,pw}}$ are the higher heating value of hydrogen, the molar flow rate of hydrogen, the solar power input for the heating requirement, and the solar power input for the penalty work requirement (see Fig. 1). The fuel output $\dot{n}_{\mathrm{H_2}}$ appearing in Eq. (4) can be expressed as:

$$\dot{n}_{\mathrm{H_2}} = (\dot{n}_{\mathrm{H_2,ox,out}} - 2\dot{n}_{\mathrm{O_2,ox,out}}) = 2(\dot{n}_{\mathrm{O_2,red,out}} - \dot{n}_{\mathrm{O_2,red,in}}) \tag{5}$$

An energy balance for the heating subsystem takes the final form:

$$\dot{Q}_{\mathrm{solar,h}} = \dot{Q}_{\mathrm{rerad}} + \dot{Q}_{\mathrm{other}} + \dot{Q}_{\mathrm{chem,WT}} + \dot{Q}_{\mathrm{sg,h}} + \dot{Q}_{\mathrm{H_2O,h}}, \tag{6}$$

where $\dot{Q}_{\text{rerad}}$, $\dot{Q}_{\text{other}}$, $\dot{Q}_{\text{chem,WT}}$, $\dot{Q}_{\text{sg,h}}$, and $\dot{Q}_{\text{H}_2\text{O,h}}$ are the re-radiation heat loss rate, the heat loss rate via conduction and convection, the heat rates to drive the water splitting, to preheat the sweep gas, and to preheat the oxidizer, respectively. The latter three terms on the right-side of Eq. (6) can be determined by:

$$\dot{Q}_{\text{chem,WT}} = \dot{n}_{\text{H}_2,\text{ox,out}} \Delta H^{\circ}_{\text{WT}}, \tag{7}$$

$$\dot{Q}_{\text{sg,h}} = \dot{n}_{\text{N}_2}[\overline{h}_{\text{N}_2}(T_5) - \overline{h}_{\text{N}_2}(T_4)] + \dot{n}_{\text{O}_2,4}[\overline{h}_{\text{O}_2}(T_5) - \overline{h}_{\text{O}_2}(T_4)], \tag{8}$$

and

$$\dot{Q}_{\text{H}_2\text{O,h}} = \dot{n}_{\text{H}_2\text{O}}[\overline{h}_{\text{H}_2\text{O}}(T_{10}) - \overline{h}_{\text{H}_2\text{O}}(T_9)], \tag{9}$$

with $\Delta H^{\circ}_{\text{WT}}$ being the standard enthalpy for the water thermolysis (WT) reaction. For the energy balance analyses of the heat exchangers ($HX_{g,red}$ and $HX_{g,ox}$) and the determination of other energy rate terms like $\dot{Q}_{\text{rerad}}$, $\dot{Q}_{\text{other}}$ and $\dot{Q}_{\text{solar,pw}}$, readers can refer to Ref. [29]. Note that the solar input for penalty work requirement $\dot{Q}_{\text{solar,pw}}$ is assumed to be independent of pressure for ranges where cryogenic separation is used and justification for this assumption can be found from Ref. [29].

The above analysis only considers the overall energy balance for the whole reactor system, leaving the mass and species conservation analyses undetermined. Mass balance analyses for non-reacting components like the heat exchangers ($HX_{g,red}$ and $HX_{g,ox}$) and the air separator (GS) are straight forward and will not be repeated. However, for the membrane reactor, both heterogeneous reduction and oxidation steps occur simultaneously under different flow configurations, making the analysis for the membrane reactor sufficiently important to warrant a section on its own.

2.2 Membrane reactor flow configurations

(*a*)

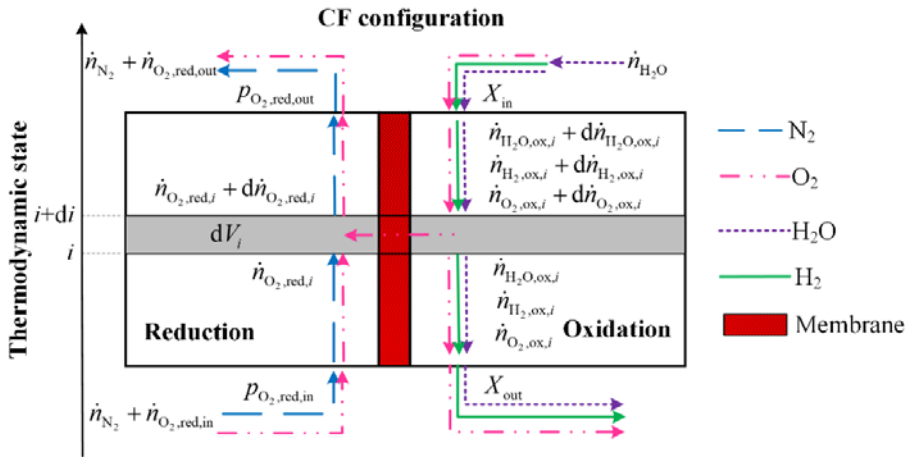

(*b*)

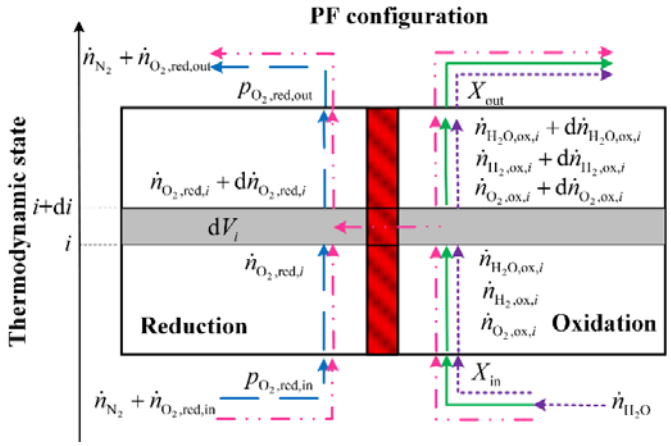

Fig. 2 Schematic of flow configurations as well as mass and species conservation for an isothermal membrane reactor under (a) CF configuration, and (b) PF configuration

Both CF and PF configurations are considered for the membrane reactor with a prescribed inlet condition of gas flow rates and thermodynamic states as shown in Fig. 2. Fig. 2(a) displays the membrane reactor operated under CF configuration and Fig. 2(b) under PF configuration. The central question regarding the mass balance analysis of the membrane reactor is:

What is the maximum outlet conversion ratio ($\max\{X_{\text{out}}\}$), and therefore the maximum fuel productivity ($\max\{\dot{n}_{\text{H}_2}\}$), under each flow configuration given prescribed inlet conditions of $\dot{n}_{\text{N}_2}$, $p_{\text{O}_2,\text{red,in}}$, $\dot{n}_{\text{H}_2\text{O}}$ and X_{in}?

The answer to this question relies on the imposition of conservation of mass and species as well as the satisfaction of Gibbs' criterion. A detailed analysis has been elaborated for a conventional redox reactor in our recent work [28], and the same methodology can be adopted for the membrane reactor case. Therefore, only the major results will be presented without a detailed derivation.

In the following analysis, we will consider the CF configuration for the case of water splitting. By imposing the conservation of species and mass for the membrane reactor we obtain:

$$\frac{\dot{n}_{\text{N}_2}}{\dot{n}_{\text{H}_2\text{O}}} = -\frac{1}{2}\frac{\text{d}X_i}{\text{d}p_i^*}, \tag{10}$$

where $p_i^* = p_{\text{O}_2,\text{red},i}\left(p_{\text{sys}} - p_{\text{O}_2,\text{red},i}\right)^{-1}$ is a dimensionless pressure. Note that the reduction gas inlet state p_{in}^* corresponds to the oxidation gas outlet state X_{out} due to the CF configuration arrangement. Integrating Eq. (10) from the reduction-inlet/oxidation-outlet point (p_{in}^*, X_{out}) to an arbitrary thermodynamic state point (p_i^*, X_i) gives

$$X_i = -2\frac{\dot{n}_{\text{N}_2}}{\dot{n}_{\text{H}_2\text{O}}}\left(p_i^* - p_{\text{in}}^*\right) + X_{\text{out}}. \tag{11}$$

Thus, a membrane reactor system that conserves mass must follow a line segment with a slope that is proportional to the flow rate ratio of nitrogen to oxidizer (known quantities for the present system) where the inlet and outlet conditions correspond to the endpoints of the mass conservation line segment.

There are five steps involved in the oxygen transport process [23,25]: (*i*) mass transfer of gaseous oxygen on the oxidation side; (*ii*) oxidation surface reaction between molecular oxygen and oxygen vacancies; (*iii*) oxygen vacancy bulk diffusion through the membrane; (*iv*) reduction surface reaction between oxygen vacancies and molecular oxygen; and (*v*) mass transfer of gaseous oxygen on the reduction side. To guarantee the oxygen transport can proceed continuously at steady state, all five steps must occur simultaneously. The mass transfer steps (*i*) and (*v*) and the bulk diffusion step (*iii*) are assumed to be fast enough as stated in our model assumptions. To ensure the reaction spontaneity of surface reaction steps *(ii*) and (*iv*), the Gibbs criterion must be satisfied. Gibbs' criterion applied to the reduction step (*iv*) takes the final form

$$\Delta G_{\mathrm{red}}(p_{\mathrm{O_2,red},i},\delta_i)=\Delta G^{\circ}_{\mathrm{red}}(T_{\mathrm{iso}},\delta_i)+\overline{R}T_{\mathrm{iso}}\ln\left(\frac{p_{\mathrm{O_2,red},i}}{p_{\mathrm{ref}}}\right)^{1/2}\le 0. \tag{12}$$

A similar relationship can be obtained for the oxidation step (*ii*) to occur spontaneously:

$$\Delta G_{\mathrm{ox,H_2O}}(X_i,\delta_i)=\Delta G^{\circ}_{\mathrm{WT}}(T_{\mathrm{iso}})+\Delta G^{\circ}_{\mathrm{ox,O_2}}(T_{\mathrm{iso}},\delta_i)+\overline{R}T_{\mathrm{iso}}\ln\frac{X_i}{1-X_i}\le 0. \tag{13}$$

Combining the inequalities of (12) and (13) via the relationship $\Delta G^{\circ}_{\mathrm{red}}(T_{\mathrm{iso}},\delta_i)=-\Delta G^{\circ}_{\mathrm{ox,O_2}}(T_{\mathrm{iso}},\delta_i)$ yields

$$\Delta G_{\mathrm{iso,mem}}(p_{\mathrm{O_2,red},i},X_i)=\Delta G^{\circ}_{\mathrm{WT}}(T_{\mathrm{iso}})+\overline{R}T_{\mathrm{iso}}\ln\frac{X_i}{1-X_i}+\overline{R}T_{\mathrm{iso}}\ln\left(\frac{p_{\mathrm{O_2,red},i}}{p_{\mathrm{ref}}}\right)^{1/2}\le 0\,. \tag{14}$$

Though Eq. (14) is derived from the metal oxide-based redox reactions, it is independent of the material thermodynamics. This is not surprising because at steady state the membrane only serves as a pure oxygen transport material. Note, however, that the membrane material must still satisfy Eqs. (12) and (13) to guarantee the steady state operation. Consequently, the overall net reaction

will be simply water thermolysis, with hydrogen generated on the oxidation side while oxygen transported across the membrane and then released on the reduction side. An alternative method to arrive at Eq. (14) can be found from **Appendix A** where Gibbs' criterion is applied to the whole reactor system.

The answer to the question posed at the beginning of this section can be formulated based on Eqs. (11) and (14). First, we state it in words:

> The maximum outlet conversion ratio corresponds to the maximum possible ordinate of the oxidation outlet point on the line segment representing conservation of mass where all points satisfy Gibbs' criterion.

This statement can then be expressed quantitatively as an optimization problem:

$$\begin{aligned} &\max \quad X_{\text{out}}\left(p_i^*, X_i\right) \\ &\text{s.t.} \quad \Delta G_{\text{iso,mem}}(p_i^*, X_i) \le 0 \ \forall\ (p_i^*, X_i) \in \{(p_i^*, X_i) : \ell_{\text{iso,mem}}(p_i^*, X_i) = 0, p_i^* \ge p_{\text{in}}^*, X_i \ge X_{\text{in}}\}, \end{aligned} \tag{15}$$

where we have defined $\ell_{\text{iso,mem}} = X_i - X_{\text{out}} + 2(\dot{n}_{\text{N}_2} / \dot{n}_{\text{H}_2\text{O}})(p_i^* - p_{\text{in}}^*)$ for convenience.

A graphical illustration of the maximization problem formulated in Eq. (15) is displayed in Fig. 3(a) for water splitting, where X_i has been plotted against p_i^* for a membrane reactor. The positions of $p_i^* = p_{\text{in}}^*$ and $X_i = X_{\text{in}}$ appearing in Fig. 3(a) are uniquely determined by the prescribed inlet conditions of the membrane reactor. The gray region satisfies the constraints appearing in Eq. (15), $\Delta G_{\text{iso,mem}} \le 0$, $p_i^* \ge p_{\text{in}}^*$, and $X_i \ge X_{\text{in}}$, and represents the desired operation region where both reduction and oxidation will proceed spontaneously. The line segments represent the possible operation of the membrane reactor such that mass is conserved, where the reduction gas inlet (p_{in}^* , X_{out}) and outlet (p_{out}^* , X_{in}) are represented by the endpoints. Different

line segments represent different levels of oxygen transport across the membrane. It can be seen that the maximum conversion ratio occurs when the mass conservation line just touches the equilibrium curve—at the point (p_{eq}^{*} , X_{eq})—yet never crosses it and stays fully within the gray area. In this example, the equilibrium state is established at some intermediate thermodynamic state.

The PF configuration can be analyzed using the same tools and arguments as were developed for the CF configuration and will not be repeated here. Instead of an optimization problem, the result can be stated as a strict equality:

$$X_{\mathrm{PF,out,max}} = X_{\mathrm{in}} + \frac{2\dot{n}_{\mathrm{N_2}}}{\dot{n}_{\mathrm{H_2O}}}(p_{\mathrm{PF,out}}^{*} - p_{\mathrm{in}}^{*}) = X_{\mathrm{eq}}(T_{\mathrm{iso}}, p_{\mathrm{PF,out}}^{*}) . \tag{16}$$

The mass conservation line representing the PF configuration for water splitting is shown in Fig. 3(b). It is obvious that the CF configuration achieves a higher $X_{\mathrm{out,max}}$ than PF for a membrane reactor under the same inlet conditions, which agrees with the conclusion drawn in our recent work [28]. This claim should hold true for all membrane materials as long as they satisfy Eqs. (12) and (13). Since ceria gratifies these criteria, we can confirm that a material capable of ideal operation of a membrane reactor exists, and the search for a membrane replacement would not lead to efficiency improvements from the thermodynamic viewpoint. The prior CF model by Tou et al. [22] and Zhu et al. [27] enforcing equilibrium at both reactor inlet and outlet is also illustrated in Fig. 3(b) for the comparison purpose; except for the two endpoints, the whole mass conservation line lies outside the meaningful operating area, implying the desired reduction and oxidation on both sides of the membrane will not occur simultaneously because Gibbs' criterion is violated. In other words, the oxygen transport through the dense membrane requires a higher partial pressure in the oxidation chamber than in the reduction chamber, which cannot be achieved based on their

models [22,27]. The above methods developed for water splitting can be readily extended to carbon dioxide splitting by simply modifying relevant thermodynamic parameters and its graphical representation is put in **Appendix B** for interested readers.

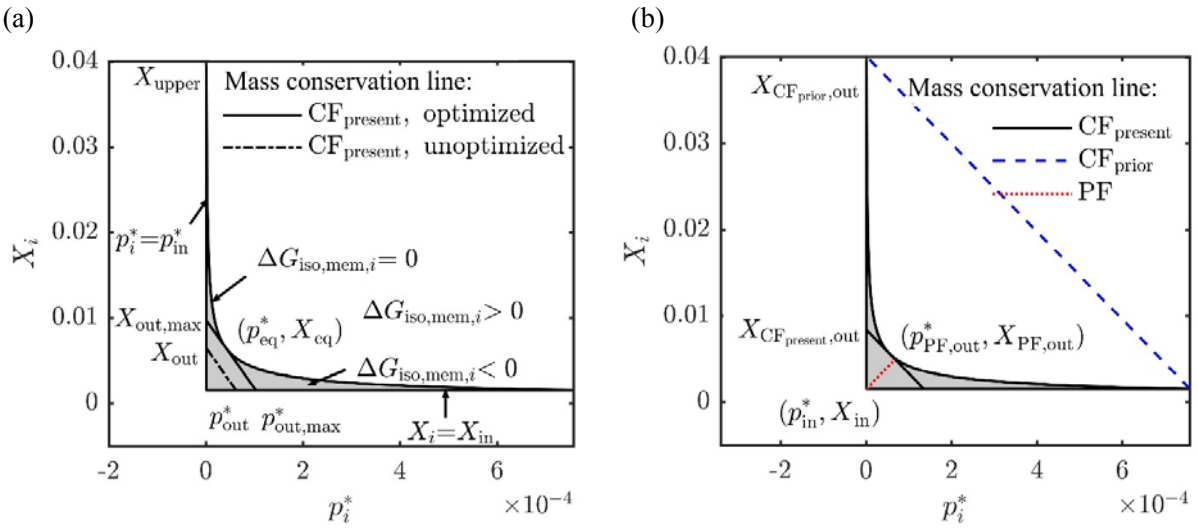

Fig. 3 A graphical representation to determine the optimal conversion ratio of an isothermal membrane reactor for water splitting given a prescribed set of inlet conditions, as detailed below. The operating conditions and values for this figure are not unique; however, they are chosen to ensure that the key features and distinction among all models under consideration are well-reflected and easy to visualize. (*a*) The present CF model of the isothermal membrane reactor at T_{iso}=1773 K with inlet conditions of $p_{in}^{*}=10^{-6}$, and $\dot{n}_{N_2}/\dot{n}_{H_2O}$ =40; and (*b*) comparison of CF and PF models of the isothermal membrane reactor at T_{iso}=1773 K with inlet conditions of $p_{in}^{*}=10^{-6}$, and $\dot{n}_{N_2}/\dot{n}_{H_2O}$ =25.5 for all models under consideration. The subscript "prior" refers to the work by Tou et al. [22] and Zhu et al. [27], and the subscript "present" refers to this work.

2.3 Simultaneous multivariable optimization

Based on the thermodynamic analyses for the whole membrane reactor system described above, the solar-to-fuel efficiency can then be determined and further optimized using the same

multivariable optimization scheme as formulated in our recent study [29]. Note that unlike the case of a conventional redox reactor system for water splitting, which contains four free parameters ($p_{\mathrm{O}_2,\mathrm{red,in}}$, $\dot{n}_{\mathrm{N}_2}/\dot{n}_{\mathrm{MO}}$, $\dot{n}_{\mathrm{H_2O}}/\dot{n}_{\mathrm{MO}}$ and T_{ox}), the membrane reactor system only yields two free parameters that can be optimized, $p_{\mathrm{O}_2,\mathrm{red,in}}$, and $\dot{n}_{\mathrm{N}_2}/\dot{n}_{\mathrm{H_2O}}$, since the reactor operates isothermally and the membrane is stationary. We use the solar-to-fuel efficiency as the objective function and state a constrained optimization problem for the membrane reactor system:

$$\begin{array}{ll} \max & \eta(p_{\mathrm{O}_2,\mathrm{red,in}}, \dot{n}_{\mathrm{N}_2}/\dot{n}_{\mathrm{H_2O}}) \\ \text{subject to} & p_{\mathrm{O}_2,\mathrm{red,L}} \le p_{\mathrm{O}_2,\mathrm{red,in}} \le p_{\mathrm{O}_2,\mathrm{red,U}},\ (\dot{n}_{\mathrm{N}_2}/\dot{n}_{\mathrm{H_2O}})_{\mathrm{L}} \le \dot{n}_{\mathrm{N}_2}/\dot{n}_{\mathrm{H_2O}} \le (\dot{n}_{\mathrm{N}_2}/\dot{n}_{\mathrm{H_2O}})_{\mathrm{U}} \end{array} \tag{17}$$

where the subscripts L and U represent lower and upper limits of these free parameters, respectively.

3. Results and discussion

Prescribed and free parameters selected for the present work are listed in Table 1 following our previous analysis [29]. These parameters apply to all results unless stated otherwise. The values of most parameters remain unchanged for convenient comparison with prior work; justification for their values can be found there [29]. The most significant differences between the present parametric study and the one found in Ref. [29] are (*i*) the absence of solid heat recovery due to the isothermal operation, (*ii*) the broader range of gas heat recovery conditions being considered, and (*iii*) the reduced number of free parameters.

In the following subsections, we first report the maximum solar-to-fuel efficiencies along with their corresponding optimal operating conditions for water splitting under both CF and PF configurations. Then the effect of each free parameter on the solar-to-fuel efficiency is investigated to elucidate which physical mechanisms lead to losses/gains in efficiency.

Table 1 Summary of prescribed and free parameters used in the thermodynamic analyses for water splitting

Parameters		Values
Prescribed	C	3000
	DNI	1000 W m^{-2}
	p_{ref}	1 atm
	p_{sys}	1 atm
	f	0.2
	$\eta_{solar\text{-}elec}$	0.25
	ε_g	0.75, 0.85, 0.95
	T_{iso}	1400–1900 K at 50 K intervals
Free	$p_{O_2,red,in}$	[10^{-6} atm, $p_{O_2,ox,in}$]
	$\dot{n}_{N_2}/\dot{n}_{H_2O}$	[0, 10^5]

3.1 Maximizing solar-to-fuel efficiency

The maximum solar-to-fuel efficiencies for water splitting under both CF and PF configurations with different gas heat recovery conditions are displayed in Fig. 4 as a function of the operating temperature. The peak solar-to-fuel efficiency for water splitting under CF and PF are 1.3% and 0.73%, respectively, and occur at T_{iso}=1900 K, ε_g=0.95. As expected, the flow configuration of CF outperforms PF in terms of solar-to-fuel efficiency under the same gas heat recovery conditions.

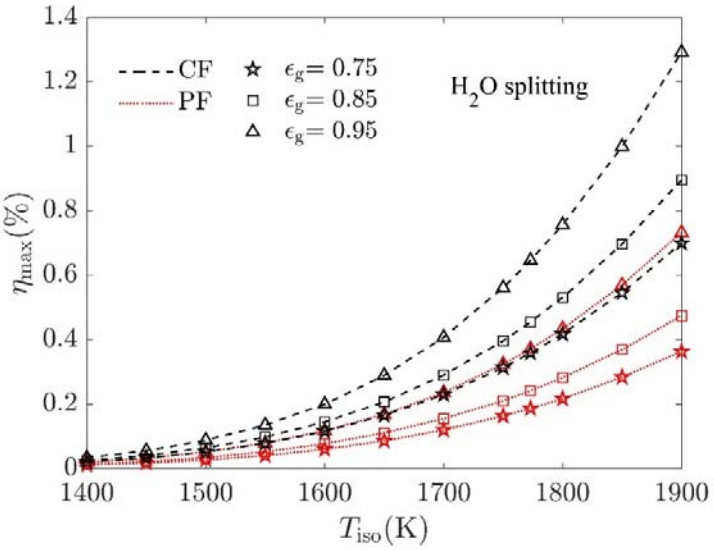

Fig. 4 Maximum solar-to-fuel efficiencies for water splitting of the membrane reactor system under CF and PF configurations with different gas heat recovery conditions

This can be understood by noting that CF achieves a higher water conversion ratio under optimal operating conditions but also at the cost of higher ratio of sweep gas to water flow rate, resulting in more fuel output as well as more solar power input. Since the former effect dominates the latter, a higher efficiency will be achieved under CF than that under PF. The peak efficiency for water splitting reported here (1.3%) for the isothermal membrane reactor system under CF configuration is indeed quite low when compared to that reported for the conventional redox reactor system under CF–CF configuration, where a peak efficiency of 11.0% is predicted at the same operating condition of T_{red}=1900 K, ε_s=0 and ε_g=0.95 [29]. This suggests that though the membrane reactor greatly simplifies the reactor design by using a stationary membrane material to realize continuous fuel production, it suffers from low efficiency. The maximum efficiencies for carbon dioxide splitting of a membrane reactor system under CF and PF configurations are 3.2% and 2.0%, respectively, at T_{iso}=1900 K, ε_g=0.95, which are higher than those for water splitting due to the

more favorable equilibrium thermodynamics of carbon dioxide splitting [4]; interested readers can refer to **Appendix C** for more detailed results.

The peak efficiencies for water splitting at T_{iso}=1900 K in Fig. 4 along with their corresponding optimal operating conditions are listed in Table 2 for both CF and PF configurations under each gas heat recovery condition. The optimal oxygen partial pressure entering the reduction side remains consistently low for both flow configurations under all gas heat recovery conditions. A general trend of lower ratio of sweep gas to water flow rates is found when the flow choice transfers from CF to PF and when the gas heat recovery condition improves.

Table 2 Peak efficiencies along with optimum operating conditions for water splitting under varying gas heat recovery conditions

Flow configurations	Optimum parameters	ε_g=0.75	ε_g=0.85	ε_g=0.95
CF	η	0.70%	0.90%	1.29%
	T_{iso} (K)	1900	1900	1900
	$p_{O_2,red,in}$ (atm)	1×10^{-6}	1×10^{-6}	1×10^{-6}
	$\dot{n}_{N_2}/\dot{n}_{H_2O}$	1.27	1.07	0.77
	X_{out}	6.6×10^{-3}	6.2×10^{-3}	5.6×10^{-3}
PF	η	0.36%	0.47%	0.73%
	T_{iso} (K)	1900	1900	1900
	$p_{O_2,red,in}$ (atm)	1×10^{-6}	1×10^{-6}	1×10^{-6}
	$\dot{n}_{N_2}/\dot{n}_{H_2O}$	1.05	0.82	0.47
	X_{out}	4.8×10^{-3}	4.6×10^{-3}	4.2×10^{-3}

We note that the maximum efficiencies for carbon dioxide splitting reported here (below 3.5% at 1900 K) under the CF configuration via multivariable optimization are much lower than those reported by Tou et al. [22] (over 35% at 1973 K) and Zhu et al. [27] (over 10% at 1800 K). Since we have demonstrated in Fig. 3(b) and Fig. 9(b) (see **Appendix B**) that their models violate Gibbs' criterion, we question their predicted efficiencies. To facilitate a fair comparison, we find Fig. S6(c) by Tou et al. [22] a more convenient reference. Herein, we revisit their work [22] using the same energy balance model while employing the revised mass balance model as developed in section 2.2 to predict the optimized efficiencies for a membrane reactor system under CF configuration. Results are displayed in Fig. 5 using their definition of efficiency [22]. The reproduction of their results confirms the employment of the same energy balance model. The revised CF model predicts much lower optimum efficiencies than their original model [22], with the highest values being 20.7% as compared to 38.3%. The difference in peak efficiencies predicted in the present study (3.2%) and the revised work of Tou et al. [22] (20.7%) can be attributed to the variation in modelling choices: (*i*) the penalty work for producing the sweep gas is considered in our work, while this has been neglected in theirs; (*ii*) the penalty work for CO_2/CO separation is determined based on different methods; (*iii*) nitrogen is employed as the sweep gas in our work while argon is used in theirs; (*iv*) an operating condition of T_{iso}=1900 K is prescribed in our model while a different condition of T_{iso}=1973 K is assumed in their work.

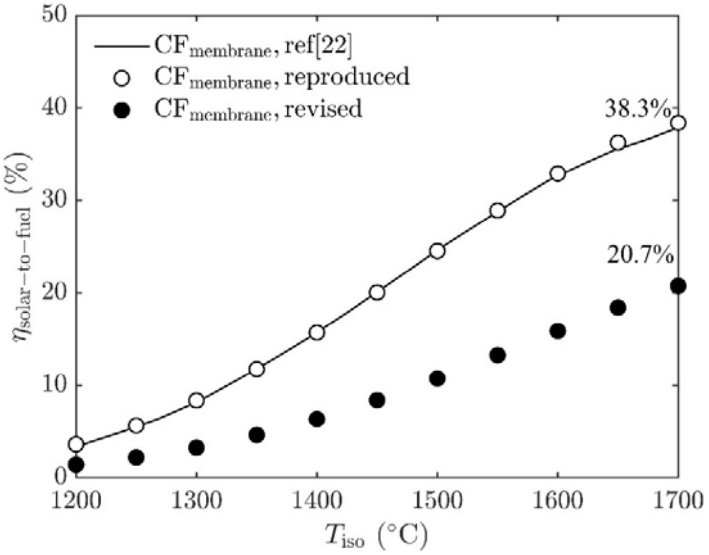

Fig. 5 Comparison of optimized efficiencies for carbon dioxide splitting with Tou et al. [22] (Fig. S6(c)) at ε_g=0.95, $p_{O_2,red,in} = 10^{-6}$ atm for an isothermal membrane reactor system operated under CF configuration. Legend text "reproduced" is in reference to the effort to reproduce the work by Tou et al. [22], and "revised" refers to using the revised CF model to revisit, modify, and optimize the work by Tou et al. [22]. The displayed values showcase the highest predicted solar-to-fuel efficiencies using the respective CF models.

Next, we examine the dominating energy requirements behind the optimal results reported above. Understanding the energetic constituents of total solar input can offer insight on reactor design and operation. To facilitate our discussion, the system power outputs are normalized by the total solar input so that their sum is 100%. This is conducted using CF configuration at the optimized case as an example to help identify the dominating energy requirements at varying temperature and gas heat recovery conditions.

An itemization of the normalized energy requirements for water splitting under CF along with the maximum efficiencies as a function of temperature under two distinct heat recovery conditions are displayed in Fig. 6, with Fig. 6(a) representing the case of ε_g=0.75 and Fig. 6(b) of ε_g=0.95.

The most dominating energy requirement is found to be the penalty work requirement for sweep gas production $\dot{Q}_{\text{solar,pw}}$, and as the gas heat recovery condition improves, its dominance becomes more significant due to the decreased heating requirement by the sweep gas $\dot{Q}_{\text{sg,h}}$ and the oxidizer $\dot{Q}_{\text{H}_2\text{O,h}}$. The energy requirement to drive the water splitting $\dot{Q}_{\text{chem,WT}}$ is relatively small compared to all other energy requirements, which consistently explains the low maximum efficiencies as displayed on the right axis in Fig. 6. Consequently, potential efficiency improvement can be achieved by increasing the solar input to fuel production and/or by reducing all other energy requirements, particularly the penalty work for sweep gas production. In light of this finding, the following efforts can be made to aim for higher efficiencies: (*i*) employing more energy-efficient sweep gas production technology or alternative oxygen partial pressure control systems such as vacuum pumping; (*ii*) improving solar reactor designs to minimize heat losses, particularly the reradiation heat loss; and (*iii*) designing more efficient high-temperature heat exchangers to further improve gas heat recovery effectiveness.

(a) (b)

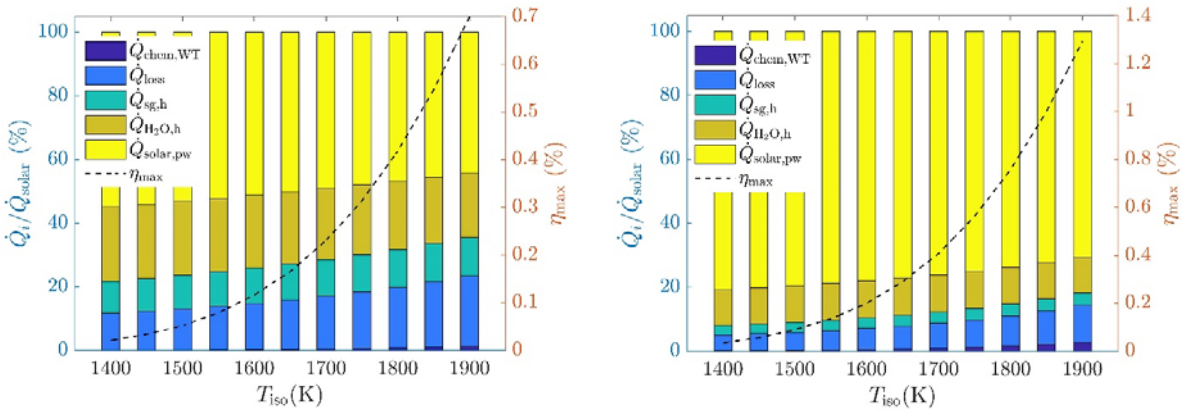

Fig. 6 Maximum solar-to-fuel efficiencies for water splitting under CF configuration along with the corresponding normalized energy requirements at varying operating temperatures with (a) ε_g=0.75, (b) ε_g=0.95

3.2 Effect of free parameters

The effect of free parameters on solar-to-fuel efficiency is investigated to elucidate how changing a certain free parameter causes deviation from the optimized efficiency conditions. The investigation is conducted considering a membrane reactor operated under CF configuration at T_{iso}=1900 K, ε_{g}=0.95. Only one free parameter is varied within a selected range while the other is held constant at the optimal value as listed in Table 2. To facilitate the analysis, the solar-to-fuel efficiency is reformulated via the introduction of dimensionless energy factor terms (F_i) following the work by Jarrett et al. [5]:

$$\eta = \frac{1}{F_{\mathrm{chem,WT}} + F_{\mathrm{loss}} + F_{\mathrm{sg,h}} + F_{\mathrm{H_2O,h}} + F_{\mathrm{solar,pw}}} \tag{18}$$

with

$$F_i = \begin{cases} \dfrac{\dot{Q}_i}{\dot{n}_{\mathrm{H_2}} \mathrm{HHV}_{\mathrm{H_2}}} & (i = \mathrm{chem,\ WT;\ sg,h;\ H_2O,h;\ solar,pw}) \\ \dfrac{\dot{Q}_{\mathrm{rerad}} + \dot{Q}_{\mathrm{other}}}{\dot{n}_{\mathrm{H_2}} \mathrm{HHV}_{\mathrm{H_2}}} & (i\text{=loss}) \end{cases} \tag{19}$$

This enables the sum of all dimensionless energy factors to be the reciprocal of the solar-to-fuel efficiency.

The effect of changes in the oxygen partial pressure entering the reduction side is illustrated in Fig. 7. The solar-to-fuel efficiency is insensitive to changes in $p_{\mathrm{O_2,red,in}}$ over a broad range and remains relatively constant within the range of 1×10^{-6}–1×10^{-4} atm, after which the efficiency begins to decrease gradually. This is not surprising since the optimal conversion ratio is always achieved over the above wide range, creating a constant high fuel output. On the other hand, the penalty work required to produce the sweep gas is assumed constant as long as cryogenic separation can be used, making the solar input also constant [29]. Once $p_{\mathrm{O_2,red,in}}$ crosses the

threshold value, both the fuel production rate and the penalty work begin to decrease due to the decreased conversion ratio and the employment of PSA for sweep gas production. A wide range of inlet partial pressures well below 1×10^{-4} atm is operable for highest reactor performance.

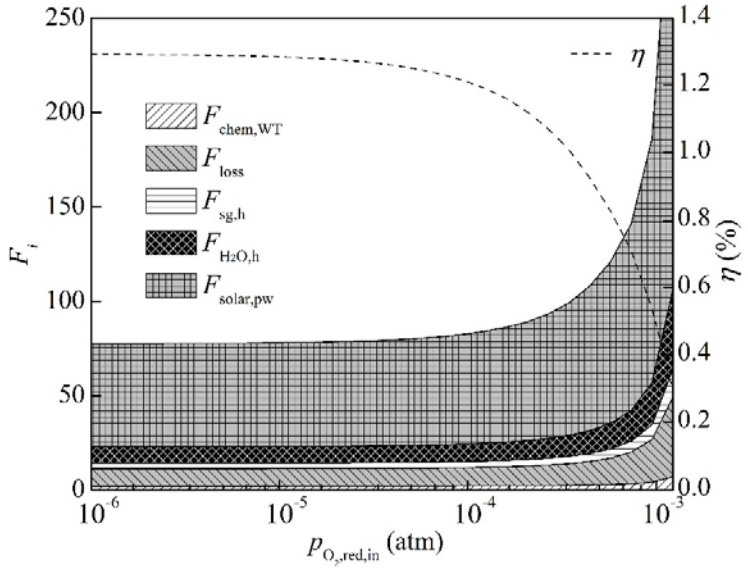

Fig. 7 Effect of oxygen partial pressure entering the reduction side on solar-to-fuel efficiency and energy constituents at T_{iso}=1900 K, ε_{g}=0.95 with $\dot{n}_{\text{N}_2}/\dot{n}_{\text{H}_2\text{O}}$ =0.77

The effect of the flow rate ratio of sweep gas to oxidizer is shown in Fig. 8. As the sweep gas flow rate increases, the oxidizer conversion ratio increases, leading to an increasing fuel output $\dot{n}_{\text{H}_2}$. Both the energy requirements to heat and produce the sweep gas ($\dot{Q}_{\text{sg,h}}$ and $\dot{Q}_{\text{solar,pw}}$) are also increased due to their proportionality to $\dot{n}_{\text{N}_2}$. The simultaneous increase in fuel output and relevant energy requirements lead to a unique maximum at an intermediate flow rate ratio value.

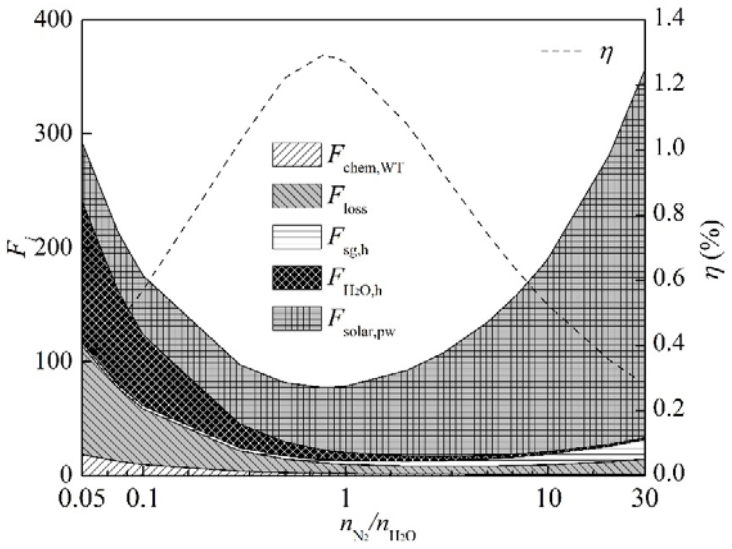

Fig. 8 Effect of sweep gas to oxidizer flow rate ratio on solar-to-fuel efficiency and energy constituents at T_{iso}=1900 K, ε_g=0.95 with $p_{O_2,red,in} = 1\times10^{-6}$ atm

4. Conclusions

A thermodynamic model based on conservation of mass and energy as well as Gibbs' criterion has been developed to predict the maximum efficiencies for a solar membrane reactor system via simultaneous optimization of all variable parameters. Peak efficiencies along with their corresponding optimal operating conditions are identified for two reactor flow configurations at varying gas heat recovery conditions. The effect of operational parameters on the solar-to-fuel efficiency has been examined.

A peak solar-to-fuel efficiency for water splitting (carbon dioxide splitting) has been found to be 1.3% (3.2%) for CF configuration and 0.73% (2.0%) for PF configuration, respectively, at operating temperature of 1900 K and 95% gas heat recovery. The CF configuration is demonstrated to be more efficient than PF under the same heat recovery conditions. In terms of the optimal operating conditions, the optimal oxygen partial pressure entering the reduction side remains consistently low (10^{-6} atm) for both flow configurations under all gas heat recovery conditions.

For the optimized case, the most dominating energy requirement has been identified to be the penalty work requirement for sweep gas production. Its share of the total solar input has been found to decrease from 55% to 44% and from 81% to 71% at ε_g=0.75 and ε_g=0.95, respectively, when the operating temperature increases from 1400 K to 1900 K. The energy requirement to drive the water splitting $\dot{Q}_{\text{chem,WT}}$ has been found to be relatively small compared to all other terms, agreeing with the low maximum efficiency result. The results reported above are found to be independent of the membrane materials as long as the continuous fuel production at steady state is guaranteed. The model results offered insights on potential efficiency improvement for membrane reactor systems that help guide future reactor designs.

Acknowledgements

The financial support of the China Scholarship Council (Sha Li, grant no. [2015]3022, 201506020092) and the Australian Research Council (Wojciech Lipiński, Future Fellowship, award no. FT140101213) is gratefully acknowledged.

Appendix A: an alternative method to derive Gibbs' criterion for the membrane reactor

An alternative method to arrive at Eq. (14) can be obtained when Gibbs' criterion is applied to the whole membrane reactor system. At steady state the membrane material only serves as a pure oxygen transport material. As a result, the overall net reaction will be simply water thermolysis, with hydrogen generated on the oxidation side and oxygen transported across the membrane and then released on the reduction side. Changes in the amount of each gaseous species are related to the stoichiometry coefficients of the overall water thermolysis reaction by:

$$-\frac{\mathrm{d}n_{\mathrm{H_2O,ox},i}}{1}=\frac{\mathrm{d}n_{\mathrm{H_2,ox},i}}{1}=\frac{\mathrm{d}n_{\mathrm{O_2,red},i}}{1/2}=\mathrm{d}\xi_{\mathrm{WT},i} \tag{A1}$$

where $\xi_{\mathrm{WT},i}$ is referred to as the local reaction extent of water thermolysis. For the whole membrane reactor system where there is no net molar change in membrane material, Gibbs' criterion takes the form of

$$\begin{aligned} \mathrm{d}G_{\mathrm{iso,mem},i}\big]_{T_{\mathrm{iso}},p_{\mathrm{sys}}} &= \mu_{\mathrm{O_2,red},i}\mathrm{d}n_{\mathrm{O_2,red},i} + \mu_{\mathrm{N_2},i}\mathrm{d}n_{\mathrm{N_2},i} \\ &+\mu_{\mathrm{O_2,ox},i}\mathrm{d}n_{\mathrm{O_2,ox},i} + \mu_{\mathrm{H_2,ox},i}\mathrm{d}n_{\mathrm{H_2,ox},i} + \mu_{\mathrm{H_2O,ox},i}\mathrm{d}n_{\mathrm{H_2O,ox},i} \le 0, \end{aligned} \tag{A2}$$

where $G_{\mathrm{iso,mem},i}\big]_{T,p}$, μ_j, and n_j are the Gibbs function of an isothermal membrane reactor system at fixed temperature and pressure, the chemical potential and the molar mass of species j (j=O_2, H_2, N_2, H_2O) in a multicomponent system, respectively, at some thermodynamic state i. Note that $\mathrm{d}n_{\mathrm{N_2},i} = 0$ because nitrogen is inert and that $\mathrm{d}n_{\mathrm{O_2,ox},i} = 0$ since it is assumed that the only oxygen crossing the membrane is caused by the oxidation/reduction of the membrane. Substituting Eq. (A1) into Eq. (A2) will yield:

$$\begin{aligned} \mathrm{d}G_{\mathrm{iso,mem},i}\big]_{T_{\mathrm{iso}},p_{\mathrm{sys}}} &= \left(\frac{1}{2}\mu_{\mathrm{O_2,red},i} + \mu_{\mathrm{H_2,ox},i} - \mu_{\mathrm{H_2O,ox},i}\right)\mathrm{d}\xi_{\mathrm{WT},i} \\ &= \left\{\Delta G^{\circ}_{\mathrm{WT}}(T_{\mathrm{iso}}) + \bar{R}T_{\mathrm{iso}}\ln\left[\frac{p_{\mathrm{H_2,ox},i}}{p_{\mathrm{H_2O,ox},i}}\left(\frac{p_{\mathrm{O_2,red},i}}{p_{\mathrm{ref}}}\right)^{1/2}\right]\right\}\mathrm{d}\xi_{\mathrm{WT},i} \le 0. \end{aligned} \tag{A3}$$

The ideal gas assumption along with the Dalton model will arrive at

$$\frac{p_{\mathrm{H_2,ox},i}}{p_{\mathrm{H_2O,ox},i}} = \frac{\dot{n}_{\mathrm{H_2,ox},i}}{\dot{n}_{\mathrm{H_2O,ox},i}} = \frac{X_i}{1-X_i}. \tag{A4}$$

Introducing Eq. (A4) into Eq. (A3) together with the relationship $\mathrm{d}\xi_{\mathrm{WT},i} > 0$ indicating the occurrence of water thermolysis will give:

$$\Delta G_{\mathrm{iso,mem},i} = \Delta G^{\circ}_{\mathrm{WT}}(T_{\mathrm{iso}}) + \bar{R}T_{\mathrm{iso}} \ln\left[\frac{X_i}{1-X_i}\left(\frac{p_{\mathrm{O_2,red},i}}{p_{\mathrm{ref}}}\right)^{1/2}\right] \le 0 \qquad \text{(A5)}$$

which is exactly equivalent to Eq. (14). This suggests that Eq. (14) or (A5) can be interpreted as the Gibbs criterion for the overall reaction of water thermolysis, with hydrogen produced on the oxidation side while oxygen permeated through the membrane and then released on the reduction side. However, since Eq. (A5) is derived based on the precondition of continuous oxygen transport at steady state, Eq. (A5) holds true only when the membrane material satisfies both Eqs. (12) and (13).

Appendix B: A graphical representation to determine the optimal conversion ratio for carbon dioxide splitting

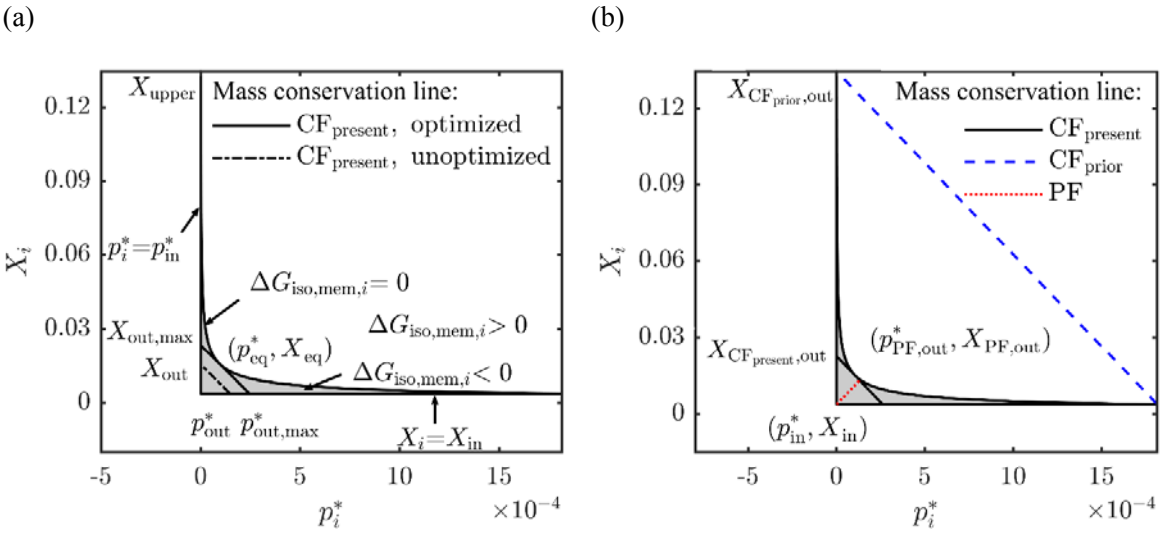

Fig. 9 A graphical representation for the determination of the optimal conversion ratio of an isothermal membrane reactor for carbon dioxide splitting given a prescribed set of inlet conditions, as detailed below. The operating conditions and values for this figure are not unique; however, they are chosen to ensure that the key features and distinction among all models under consideration are well-reflected and easy to visualize. (*a*) The present CF model for the isothermal membrane reactor

at T_{iso}=1773 K with inlet conditions of $p_{in}^{*}=10^{-6}$, and $\dot{n}_{N_2}/\dot{n}_{CO_2}$ =40; and (*b*) comparison of CF and PF models of the isothermal membrane reactor at T_{iso}=1773 K with inlet conditions of $p_{in}^{*}=10^{-6}$, and $\dot{n}_{N_2}/\dot{n}_{CO_2}$ =36.0 for all models under consideration. The subscript "prior" refers to the work by Tou et al. [22] and Zhu et al. [27], and the subscript "present" refers to this work.

Appendix C: maximum solar-to-fuel efficiencies for carbon dioxide splitting

The maximum solar-to-fuel efficiencies of the membrane reactor system for carbon dioxide splitting as a function of the operating temperature at varying gas recovery conditions are shown in Fig. 10 under both CF and PF configurations. Unlike the case of water splitting, the penalty work for carbon dioxide splitting includes two contributions: (*i*) the air separation work for sweep gas production required in the reduction chamber; (*ii*) the product separation work of carbon monoxide from the product mixtures. Readers can refer to Ref. [29] for detailed description.

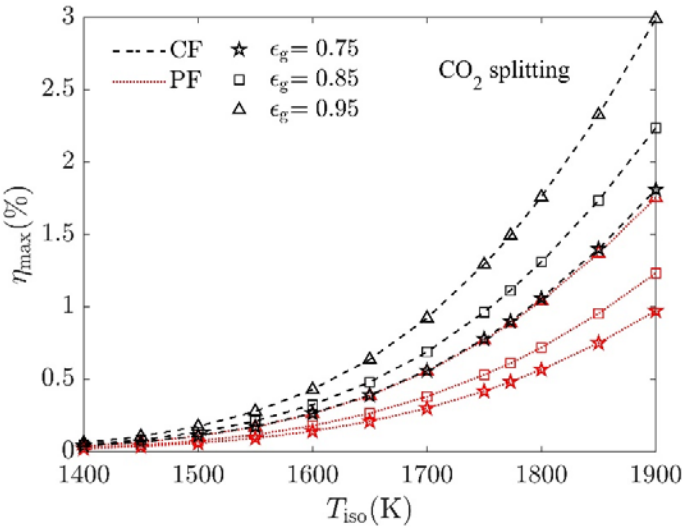

Fig. 10 Maximum solar-to-fuel efficiencies for carbon dioxide splitting of the membrane reactor system under CF and PF configurations with different gas heat recovery conditions

Nomenclature

A_{aperture}=aperture area of reactor, m^2

C= solar concentration ratio

DNI=direct normal irradiance, W m^{-2}

dV=a differential control volume, m^3

f=conduction and convection heat losses factor

F=dimensionless energy factor introduced in Eq. (18)

$\overline{h}$ =molar enthalpy, J mol^{-1}

HHV= higher heating value, J mol^{-1}

$\dot{n}$ =molar flow rate, mol s^{-1}

p=pressure, atm

p^* =dimensionless pressure as defined by $p_i^* = p_{\mathrm{O}_2,\mathrm{red},i}\left(p_{\mathrm{sys}} - p_{\mathrm{O}_2,\mathrm{red},i}\right)^{-1}$

$\dot{Q}$ =heat rate, W

$\overline{R}$ = universal molar gas constant, 8.314 J mol^{-1} K^{-1}

$\overline{s}$ = molar entropy, J mol^{-1} K^{-1}

T=temperature, K

$\overline{w}$ =molar separation work, J mol^{-1}

$\dot{W}$ =work rate, W

X=conversion ratio

Greek Symbols

$\Delta G_{\text{iso,mem}}$ = change in Gibbs function for isothermal membrane reactor, J mol^{-1}

$\Delta G^{\circ}_{ox,H_2O}$ = standard molar Gibbs free energy for oxidation with water, J mol^{-1}

$\Delta G^{\circ}_{ox,O_2}$ = standard molar Gibbs free energy for oxidation with oxygen, J mol^{-1}

ΔG°_{red} = standard molar Gibbs free energy for reduction reaction, J mol^{-1}

ΔG°_{WT} = standard molar Gibbs free energy for WT reaction, J mol^{-1}

ΔH°_{ox} = standard molar enthalpy for oxidation with oxygen, J mol^{-1}_{O}

ΔH°_{red} = standard molar enthalpy for reduction reaction, J mol^{-1}_{O}

ΔH°_{WT} =standard molar enthalpy for WT reaction, J mol^{-1}

ΔS°_{ox} = standard molar entropy for oxidation with oxygen, J K^{-1} mol^{-1}_{O}

ΔS°_{red} = standard molar entropy for reduction, J K^{-1} mol^{-1}_{O}

$\Delta\delta$ =non-stoichiometry swing

ΔT =temperature swing, K

δ =non-stoichiometry

μ_j = chemical potential of species j, J mol^{-1}

ε =heat recovery effectiveness

η =solar-to-fuel efficiency

$\eta_{solar\text{-}elec}$ =solar-to-electricity efficiency

σ =Stefan–Boltzmann constant, W m^{-2} K^{-4}

Subscripts

1,2…=thermodynamic state point

amb=ambient condition

chem,WT=chemical reaction of water thermolysis

eq=equilibrium condition

g=gas phase

h=heating requirement

i=thermodynamic state

in=inlet

iso=isothermal

iso,mem=isothermal membrane reactor

L=lower limit

max=maximum

MO=metal oxide

other=other heat losses mode

out=outlet

ox=oxidation

ox,H_2O=oxidation reaction with steam as given by Eq.(2)

ox,O_2=oxidation reaction with oxygen

pw=penalty work

red=reduction

ref=reference condition

rerad=reradiation heat loss

s=solid phase

sg=sweep gas

solar=solar heat rate input

sys=system

U=upper limit

Superscripts

◦=standard condition at T and p_{atm}

Abbreviations

CF=countercurrent flow

GS=gas separator

HX=heat exchanger

MO=metal oxide

OPM=oxygen permeation material

PF=parallel flow

PSA=pressure swing adsorption

WT=water thermolysis

References

[1] Chueh, W. C., Falter, C., Abbott, M., Scipio, D., Furler, P., Haile, S. M., and Steinfeld, A., 2010, "High-Flux Solar-Driven Thermochemical Dissociation of CO_2 and H_2O Using Nonstoichiometric Ceria," Science, 330(6012), pp. 1797–1801.

[2] Romero, M., Steinfeld, A., 2012, "Concentrating solar thermal power and thermochemical fuels," Energy & Environmental Science, 5(11), 9234.

[3] Lapp, J., Davidson, J. H., Lipiński, W., 2012, "Efficiency of two-step solar thermochemical non-stoichiometric redox cycles with heat recovery," Energy, 37(1), pp. 591–600.

[4] Krenzke, P. T., Davidson, J. H., 2015, "On the Efficiency of Solar H_2 and CO Production via the Thermochemical Cerium Oxide Redox Cycle: The Option of Inert-Swept Reduction," Energy & Fuels, 29(2), pp. 1045–1054.

[5] Jarrett, C., Chueh, W., Yuan, C., Kawajiri, Y., Sandhage, K. H., Henry, A., 2016, "Critical limitations on the efficiency of two-step thermochemical cycles," Solar Energy, 123, pp. 57–73.

[6] Ermanoski, I., Miller, J. E., Allendorf, M. D., 2014, "Efficiency maximization in solar-thermochemical fuel production: challenging the concept of isothermal water splitting," Physical chemistry chemical physics : PCCP, 16(18), pp. 8418–8427.

[7] Marxer, D., Furler, P., Takacs, M., Steinfeld, A., 2017, "Solar thermochemical splitting of CO_2 into separate streams of CO and O_2 with high selectivity, stability, conversion, and efficiency," Energy & Environmental Science, 10(5), pp. 1142–1149.

[8] Bader, R., Venstrom, L. J., Davidson, J. H., Lipiński, W., 2013, "Thermodynamic Analysis of Isothermal Redox Cycling of Ceria for Solar Fuel Production," Energy & Fuels, 27(9), pp. 5533–5544.

[9] Venstrom, L. J., De Smith, R. M., Hao, Y., Haile, S. M., Davidson, J. H., 2014, "Efficient Splitting of CO_2 in an Isothermal Redox Cycle Based on Ceria," Energy & Fuels, 28(4), pp. 2732–2742.

[10] Muhich, C. L., Evanko, B. W., Weston, K. C., Lichty, P., Liang, X., Martinek, J., Musgrave, C. B., and Weimer, A. W., 2013, "Efficient generation of H_2 by splitting water with an isothermal redox cycle," Science, 341(6145), pp. 540–542.

[11] Kong, H., Hao, Y., Jin, H., 2018, "Isothermal versus two-temperature solar thermochemical fuel synthesis: A comparative study," Applied Energy, 228, pp. 301–308.

[12] Al-Shankiti, I., Ehrhart, B. D., Weimer, A. W., 2017, "Isothermal redox for H_2O and CO_2 splitting—A review and perspective," Solar Energy, 156, pp. 21–29.

[13] Roeb, M., Neises, M., Säck, J.-P., Rietbrock, P., Monnerie, N., Dersch, J., Schmitz. M., and Sattler, C., 2009, "Operational strategy of a two-step thermochemical process for solar hydrogen production," International Journal of Hydrogen Energy, 34(10), pp. 4537–4545.

[14] Furler, P., Scheffe, J., Gorbar, M., Moes, L., Vogt, U., Steinfeld, A., 2012, "Solar Thermochemical CO_2 Splitting Utilizing a Reticulated Porous Ceria Redox System," Energy & Fuels, 26(11), pp. 7051–7059.

[15] Lapp, J., Lipiński, W., 2014, "Transient Three-Dimensional Heat Transfer Model of a Solar Thermochemical Reactor for H_2O and CO_2 Splitting Via Nonstoichiometric Ceria Redox Cycling," Journal of Solar Energy Engineering, 136(3), 031006.

[16] Ermanoski, I., Siegel, N. P., Stechel, E. B., 2013, "A New Reactor Concept for Efficient Solar-Thermochemical Fuel Production," Journal of Solar Energy Engineering, 135(3), 031002.

[17] Diver, R. B., Miller, J. E., Allendorf, M. D., Siegel, N. P., Hogan, R. E., 2008, "Solar Thermochemical Water-Splitting Ferrite-Cycle Heat Engines," Journal of Solar Energy Engineering, 130(4), 041001.

[18] Fletcher, E. A., Moen, R. L., 1977, "Hydrogen-and oxygen from water," Science, 197(4308), pp. 1050–1056.

[19] Browall, K., Doremus, R., 1977, "Synthesis and Evaluation of Doped Y_2O_3-Stabilized ZrO_2 for the Production of Hydrogen," Journal of the American Ceramic Society, 60(5-6), pp. 262–267.

[20] Naito, H., Arashi, H., 1995, "Hydrogen production from direct water splitting at high temperatures using a ZrO_2-TiO_2-Y_2O_3 membrane," Solid State Ionics, 79, pp. 366–370.

[21] Wang, H., Hao, Y., Kong, H., 2015, "Thermodynamic study on solar thermochemical fuel production with oxygen permeation membrane reactors," International Journal of Energy Research, 39(13), pp. 1790–1799.

[22] Tou, M., Michalsky, R., Steinfeld, A., 2017, "Solar-Driven Thermochemical Splitting of CO_2 and In Situ Separation of CO and O_2 across a Ceria Redox Membrane Reactor," Joule, 1(1), pp. 146–154.

[23] Xu, S. J., Thomson, W. J., 1999, "Oxygen permeation rates through ion-conducting perovskite membranes," Chemical Engineering Science, 54(17), pp. 3839–3850.

[24] Tan, X., Li, K., 2002, "Modeling of air separation in a LSCF hollow-fiber membrane module," AIChE journal, 48(7), pp. 1469–1477.

[25] Wu, X. Y., Ghoniem, A. F., 2018, "Hydrogen-assisted Carbon Dioxide Thermochemical Reduction on $La_{0.9}Ca_{0.1}$ $FeO_{3-\delta}$ Membranes: A Kinetics Study," ChemSusChem, 11(2), pp. 483–493.

[26] Wu, X.-Y., Ghoniem, A. F., 2018, "CO_2 reduction and methane partial oxidation on surface catalyzed $La_{0.9}$ $Ca_{0.1}FeO_{3-\delta}$ oxygen transport membranes," Proceedings of the Combustion Institute (epub).

[27] Zhu, L., Lu, Y., Shen, S., 2016, "Solar fuel production at high temperatures using ceria as a dense membrane," Energy, 104, pp. 53–63.

[28] Li, S., Wheeler, V. M., Kreider, P. B., Lipiński, W., 2018, "Thermodynamic Analyses of Fuel Production via Solar-Driven Non-stoichiometric Metal Oxide Redox Cycling. Part 1. Revisiting Flow and Equilibrium Assumptions," Energy & Fuels, 32(10), pp. 10838–10847.
[29] Li, S., Wheeler, V. M., Kreider, P. B., Bader, R., Lipiński, W., 2018, "Thermodynamic Analyses of Fuel Production via Solar-Driven Non-stoichiometric Metal Oxide Redox Cycling. Part 2. Impact of Solid–Gas Flow Configurations and Active Material Composition on System-Level Efficiency," Energy & Fuels, 32(10), pp. 10848–10863.

Table caption list

Table 1 Summary of prescribed and free parameters used in the thermodynamic analyses for water splitting

Table 2 Peak efficiencies along with optimum operating conditions for water splitting under varying gas heat recovery conditions

Figure caption list

Fig. 1 Schematic of mass and energy flow of an isothermal membrane reactor system under the CF configuration for water splitting. Mass flow is indicated by thin arrows and energy flow by thick, gray arrows. An energy flow line pointing to or from a mass flow line indicates a heat addition or removal step, respectively.

Fig. 2 Schematic of flow configurations as well as mass and species conservation for an isothermal membrane reactor under (a) CF configuration, and (b) PF configuration

Fig. 3 A graphical representation to determine the optimal conversion ratio of an isothermal membrane reactor for water splitting given a prescribed set of inlet conditions, as detailed below. The operating conditions and values for this figure are not unique; however, they are chosen to ensure that the key features and distinction among all models under consideration are well-reflected and easy to visualize. (*a*) The present CF model of the isothermal membrane reactor at T_{iso}=1773 K with inlet conditions of $p_{in}^{*} = 10^{-6}$, and

$\dot{n}_{N_2}/\dot{n}_{H_2O}$ =40; and (*b*) comparison of CF and PF models of the isothermal membrane reactor at T_{iso}=1773 K with inlet conditions of $p_{in}^{*}=10^{-6}$, and $\dot{n}_{N_2}/\dot{n}_{H_2O}$ =25.5 for all models under consideration. The subscript "prior" refers to the work by Tou et al. [22] and Zhu et al. [27], and the subscript "present" refers to this work.

Fig. 4 Maximum solar-to-fuel efficiencies for water splitting of the membrane reactor system under CF and PF configurations with different gas heat recovery conditions

Fig. 5 Comparison of optimized efficiencies for carbon dioxide splitting with Tou et al. [22] (Fig. S6(c)) at ε_g=0.95, $p_{O_2,red,in}=10^{-6}$ atm for an isothermal membrane reactor system operated under CF configuration. Legend text "reproduced" is in reference to the effort to reproduce the work by Tou et al. [22], and "revised" refers to using the revised CF model to revisit, modify, and optimize the work by Tou et al. [22]. The displayed values showcase the highest predicted solar-to-fuel efficiencies using the respective CF models.

Fig. 6 Maximum solar-to-fuel efficiencies for water splitting under CF configuration along with the corresponding normalized energy requirements at varying operating temperatures with (a) ε_g=0.75, (b) ε_g=0.95

Fig. 7 Effect of oxygen partial pressure entering the reduction side on solar-to-fuel efficiency and energy constituents at T_{iso}=1900 K, ε_g=0.95 with $\dot{n}_{N_2}/\dot{n}_{H_2O}$ =0.77

Fig. 8 Effect of sweep gas to oxidizer flow rate ratio on solar-to-fuel efficiency and energy constituents at T_{iso}=1900 K, ε_g=0.95 with $p_{O_2,red,in}=1\times10^{-6}$ atm

Fig. 9 A graphical representation for the determination of the optimal conversion ratio of an isothermal membrane reactor for carbon dioxide splitting given a prescribed set of inlet

conditions, as detailed below. The operating conditions and values for this figure are not unique; however, they are chosen to ensure that the key features and distinction among all models under consideration are well-reflected and easy to visualize. (*a*) The present CF model for the isothermal membrane reactor at T_{iso}=1773 K with inlet conditions of $p_{in}^{*}=10^{-6}$, and $\dot{n}_{N_2}/\dot{n}_{CO_2}$ =40; and (*b*) comparison of CF and PF models of the isothermal membrane reactor at T_{iso}=1773 K with inlet conditions of $p_{in}^{*}=10^{-6}$, and $\dot{n}_{N_2}/\dot{n}_{CO_2}$ =36.0 for all models under consideration. The subscript "prior" refers to the work by Tou et al. [22] and Zhu et al. [27], and the subscript "present" refers to this work.

Fig. 10 Maximum solar-to-fuel efficiencies for carbon dioxide splitting of the membrane reactor system under CF and PF configurations with different gas heat recovery conditions